A first generation compact microbeam radiation therapy system based on carbon nanotube X-ray technology

M. Hadsell,[1,a)] J. Zhang,[1,2] P. Laganis,[3] F. Sprenger,[3] J. Shan,[1] L. Zhang,[4] L. Burk,[1] H. Yuan,[5] S. Chang,[1,2] J. Lu,[1,4] and O. Zhou[1,4,b)]

[1]*Department of Physics and Astronomy, University of North Carolina, Chapel Hill, North Carolina 27599, USA*
[2]*Department of Radiation Oncology, University of North Carolina, Chapel Hill, North Carolina 27599, USA*
[3]*XinRay Systems, Inc., 7020 Kit Creek Road, Suite 210, Research Triangle Park, North Carolina 27709, USA*
[4]*Curriculum in Applied and Materials Sciences, University of North Carolina, Chapel Hill, North Carolina 27599, USA*
[5]*Biomedical Research Imaging Center, University of North Carolina, Chapel Hill, North Carolina 27599, USA*

(Received 5 June 2013; accepted 22 September 2013; published online 30 October 2013)

We have developed a compact microbeam radiation therapy device using carbon nanotube cathodes to create a linear array of narrow focal line segments on a tungsten anode and a custom collimator assembly to select a slice of the resulting wedge-shaped radiation pattern. Effective focal line width was measured to be 131 μm, resulting in a microbeam width of $\sim$300 μm. The instantaneous dose rate was projected to be 2 Gy/s at full-power. Peak to valley dose ratio was measured to be $>$17 when a 1.4 mm microbeam separation was employed. Finally, multiple microbeams were delivered to a mouse with beam paths verified through histology. © *2013 AIP Publishing LLC*. [http://dx.doi.org/10.1063/1.4826587]

More than half of cancer patients in North America rely on radiation therapy (RT) as part of their treatment plan.[1] The primary goal of RT, like other cancer treatments, is to eliminate the cancer while preventing simultaneous and intolerable damage to the surrounding normal tissues.[2] Although incredible strides to this end have recently been made through the use of increasingly conformal techniques and much stronger targeting, no such technique has succeeded in leaving normal tissue completely unscathed while eradicating the targeted tumor.[3] A recent modality of RT called microbeam radiation therapy (MRT), however, has in the past two decades shown promise in achieving complete normal tissue sparing during the treatment of deep-seated brain tumors in rats.[4] In one of the earlier studies, it was shown that MRT can increase the lifespan of brain tumor-bearing rats by up to a factor of ten through total tumor ablation,[5] and more recently, it has also been suggested that this technique could be used to treat neurological disease based on its ability to create microscopic, radiosurgical brain lesions in rats.[6]

The history of MRT is rooted in two research areas initially explored more than half a century ago. The purpose of the first was to determine the morbidity of the ultra-high dose heavy-ion pencil beams present in space expeditions.[7] In these studies, it was found that microscopically small beams ($\sim$25 μm) could deposit doses of up to 4000 Gy without causing tissue-level damage,[8] the discovery of which led to the use of such microbeams for cell-specific radiobiological research.[9] The second was the use of spatially fractionated, or GRID, radiation therapy to treat target areas with a macroscopic, checkerboard-like pattern of radiation.[10] This technique was initially developed before the advent of megavoltage therapy to spare skin during the treatment of deep-seated tumors with orthovoltage X-rays.[11] More recently, single fractions of megavoltage GRID therapy achieved through the use of large sieve-type blocks or multileaf collimators (MLCs)[12] have been shown to effectively augment conventional radiotherapy, providing the extra tumor dose necessary for the complete clinical and pathological control of large and bulky tumors.[13]

MRT combines the working concepts of these two areas of research by employing arrays of microscopically-thin ($\sim$100 μm), planar X-ray beams that are separated by several times their beam width.[14] The resulting radiation dose distribution has characteristic peaks and valleys with an extremely high ($>$10) peak to valley dose ratio (PVDR).[15] Retaining this high PVDR has been shown to be essential[16] to sparing developing normal brain tissue in weaning piglets,[17] duck embryos,[18] and suckling rats.[19] The megavoltage photon energies used in most conventional RT cannot be used for MRT due to the fact that the ranges of the scattered, secondary charged particles created in the tissue are far too great to preserve the microbeam pattern.[20] Moreover, it has been found that extremely large peak doses ($>$100 Gy) are required in order to completely ablate the aggressive tumors for which this technique would be best-suited.[21] Obtaining such high doses is unattainable within feasible time scales using conventional orthovoltage X-ray tubes. This is due to the fact that their dose rate would either be far too small in the case of micro-focus tubes,[22] or prohibitively reduced by microbeam collimation in the case of tubes with typically sized (between 1 mm and 10 mm) focal spots.[23] As a result, MRT has only been studied at synchrotron facilities, where the creation of ultra-high flux, orthovoltage, and parallel X-ray beams is readily achievable.[24]

The sparseness of synchrotron sources has limited the availability of MRT research to the greater scientific community. Partly because of this, the radiobiological reasons

[a)]Electronic addresses: mhadsell@stanford.edu and michadsell@gmail.com
[b)]Electronic mail: zhou@email.unc.edu

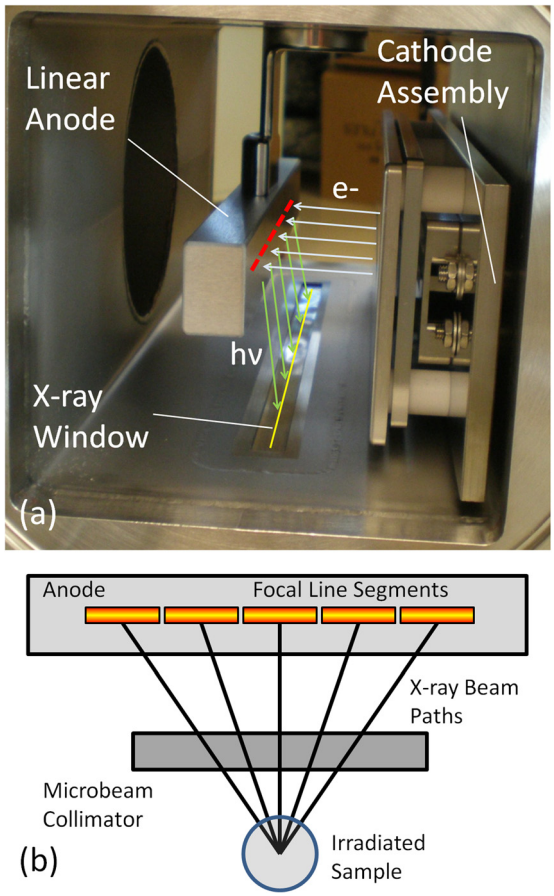

FIG. 1. (a) Photograph detailing the basic structure inside the compact microbeam irradiator Also shown are indicators for electron trajectories from the cathode assembly (light blue), the location of the segmented focal line on the anode (red), X-ray photon trajectories from the anode (light green), and the projected focal line image on the window (yellow). (b) Diagram (as seen from cathode assembly) showing how the multiple line segments produce microbeam paths that irradiate a sample from different angles. For another illustration of how microbeams are created from our source, see Figure 4(b).

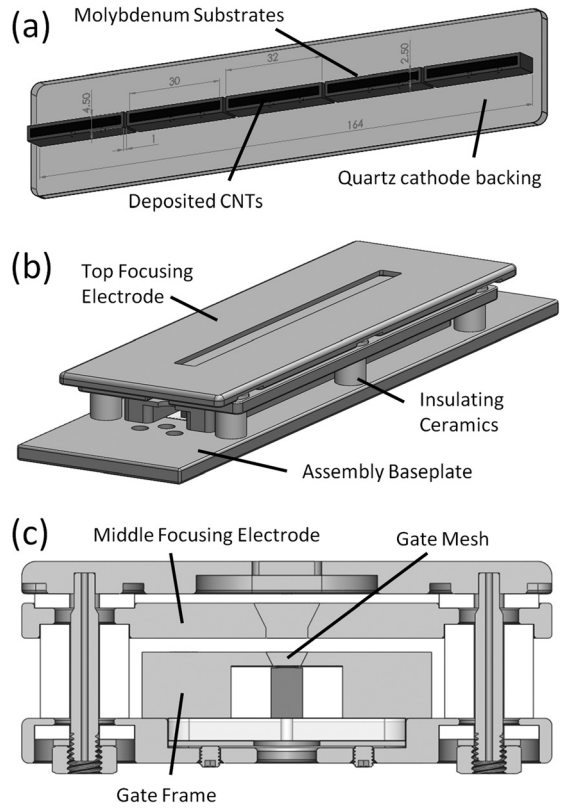

FIG. 2. (a) Solidworks™ diagram showing linear array of cathodes used in the compact MRT device. (b) Diagram illustrating the entire cathode assembly and the linear focusing track. (c) Cross section through the assembly showing the internal components and the focusing geometry used.

behind this effect are still largely unknown.[25] There is a clear need to create microbeam dose distributions with a smaller footprint at a lower cost, so as to spread and accelerate the research on this promising therapy technique and, optimally, to translate it to clinics for patient treatment. Here we report a compact and high power microbeam irradiator for treatment of tumor bearing small animals that is enabled by our unique carbon nanotube (CNT) field emission X-ray array technology.[26] This device, as illustrated in Figure 1, uses a linear array of CNT cathodes to create a line-focused X-ray source with a long (162 mm) and narrow (0.14 mm) focal track to deliver a higher microbeam dose rate than what is afforded by a micro-focus point x-ray source and to provide an improved depth dose profile during conformal radiation delivery. Here we report the design and performance of this compact microbeam irradiator.

The two primary components of the CNT MRT system that make it unique are the linear cathode array and the collimator alignment system. The array, as seen in Figure 2(a), is made up five molybdenum substrates with CNTs deposited on each of their surfaces in a 2.5 mm × 30 mm area by the electrophoretic deposition method as described previously.[27] The linear, dual-electrode focusing track and gate mesh, as illustrated in Figures 2(b) and 2(c), constitutes a three-component Einzel lens whose structure was simulated by a commercial software package (Opera 3D Vector Fields Software, Cobham plc, Dorset, UK) to be capable of focusing the electrons

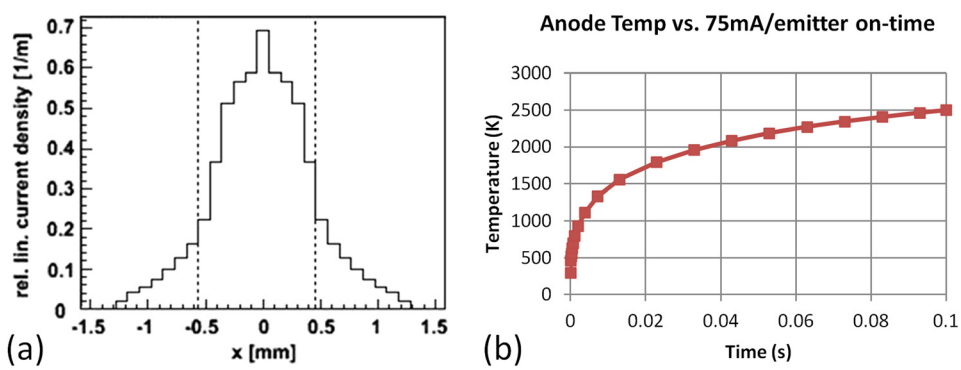

FIG. 3. (a) Simulation results displaying 1.02 mm focal line width given the geometrical setup of our cathode assembly and focusing structure. (b) Graph displaying maximum anode temperature given five simultaneous 75 mA pulses of varying widths. Note that the maximum temperature reached using a 0.1 ms pulse is well below the melting temperature of molybdenum.

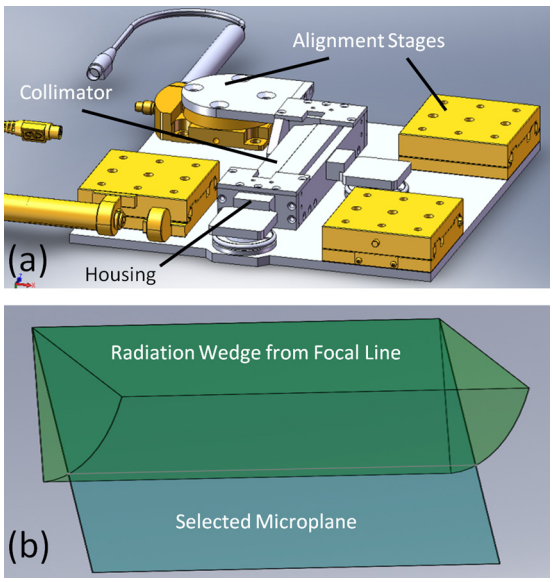

FIG. 4. (a) Solidworks™ diagram showing the structure of the collimator alignment system. Notice the rotational and translational degrees of freedom necessary for alignment. (b) Diagram illustrating how the collimator selects out a microplane from the wedge of radiation that emanates from the focal line. The angle of this wedge to the face of the anode is set by angle blocks holding the collimator within its housing.

extracted from each cathode into a 1.02 mm × 30 mm focal line segment on the anode, as illustrated in Figure 3(a).[28] The anode itself is made up of a 17 mm × 25 mm × 222 mm block of molybdenum whose front 25 mm × 222 mm surface was sputtered with a 200 μm layer of tungsten and mirror finished for ideal and uniform X-ray production. This anode was simulated using Ansys® Finite Element Analysis software (Ansys, Canonsburg, PA) to be able to withstand up to 75 mA of current per focal line segment in short pulses of 0.1 s without reaching either the melting point of the tungsten (3683 K) or the molybdenum (2890 K), as plotted in Figure 3(b).[29]

The collimator alignment system, as shown in Figure 4(a), aligns a 175 μm slit in a 9 mm thick and 150 mm long collimator to the 162 mm long focal line. The slit, made from two tungsten carbide parallels clamped against glass spacers, was statically positioned at an 8° to the anode surface by angled blocks in the collimator housing and aligned to the focal line using an assortment of micrometrically precise translation and rotation stages from the Newport Corporation (Irvine, CA). These stages are arranged in a flattened configuration to allow samples to be as close as possible to the source. In order to determine the actual alignment, an X-ray camera from Hamamatsu Photonics (Hamamatsu, Japan) and a custom alignment protocol developed at UNC are used to find the focal line through the collimator and fine-tune stage positioning. As illustrated in Figure 4(b), the 8° collimator angle effectively sets the projection angle by selecting a plane in the wedge of radiation emanating from the focal line, and thus defines the simulated effective focal line width to be 142 μm.

After construction, the device was characterized for focal line shape and cathode current stability. The average focal line segment width was measured using a method adapted from the European standard (EN 12543-5) (Ref. 30) for determining the dimensions of focal spots in micro-focus X-ray tubes. Our modification of the standard employed a single 6 in. long, 1 mm diameter tungsten wire phantom and its image on an X-ray camera to make a measurement of the focal line width using the magnification and sharpness of the image. The focal line width of the electron beam on the anode surface was measured to be 0.94 ± 0.07 mm based on an average of the measurement over all five line segments, agreeing well with the simulated value of 1.02 mm. This results in a measured effective focal line width of 131 μm at the selected projection angle of 8°. The cathode current also behaved stably over time, showing almost negligible degradation over multiple days of use, as shown in Figure 5. This data was taken over four days and fifteen hours of use. Notice that the voltage necessary to produce 46.5 mA cathode current (30 mA tube current given a measured cathode-gate transmission rate of 65%) increases more within any one day of use than it does between consecutive days. This is due to device heating that causes increased resistance in the system during long irradiations.

As a demonstration of the output of the prototype system, preliminary estimates of the peak microbeam dose rate

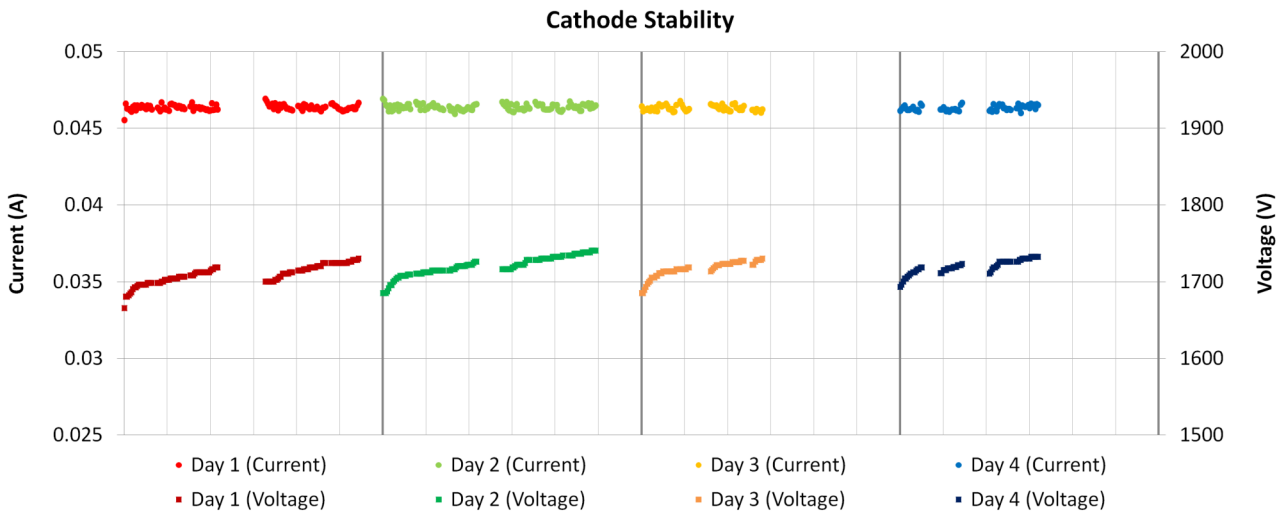

FIG. 5. Graph displaying cathode stability over multiple days of use with horizontal axis divided into hours for each day. Notice that the voltage required to produce a constant 46.5 mA of cathode current does not appreciably change between days and only increases during usage, recovering after long breaks in use.

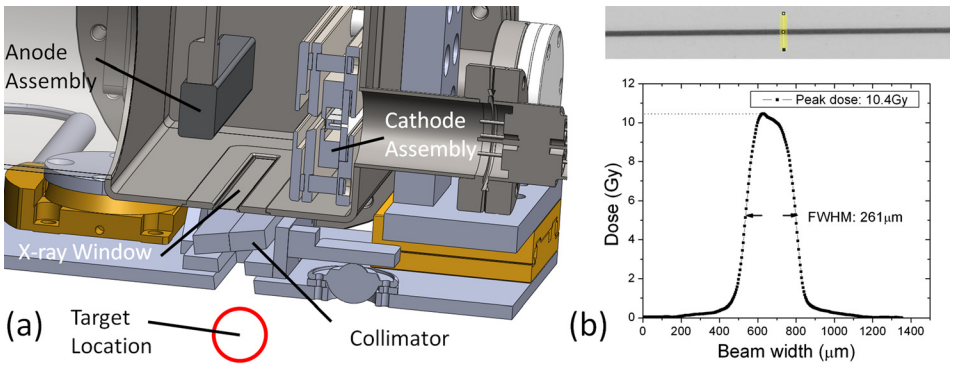

FIG. 6. (a) Solidworks™ cross section of the entire device design displaying the target location beneath the anode, X-ray window, and collimator assemblies. (b) Sample irradiated film and beam profile displaying the peak dose achieved in 8 min of irradiation and width of the microbeam created.

and PVDR of a sample microbeam pattern were attained. Gafchromic EBT2 film (Ashland Advanced Materials, Covington, KY) was adopted for these initial measurements of the CNT microbeam radiation source due to its quoted dose range between 0 and 40 Gy in the green channel, high spatial resolution, and energy independence from about 60 keV into the MeV range.[31] For our microbeam study, the film calibration curve was created using the 6 MV X-ray beam from a clinical Cyberknife® (Accuray, Sunnyvale, CA) source installed in the Radiation Oncology Department of the North Carolina Cancer Hospital. All dose film scans were performed according to the recommendations of Ashland, Inc., using a Perfection V700 flatbed scanner (Epson America, Long Beach, CA).[32]

In order to estimate the maximum peak entrance dose rate that a small animal placed in the treatment would experience, a strip of film was placed directly beneath the collimator alignment system, as shown in Figure 6(a). The compact MRT device was operated at a constant anode voltage of 160 kV, while given a tube current of 70 mA from a single cathode driven at a 1 ms pulse width and 5% duty cycle for approximately 8 min. As can be seen in Figure 6(b), the peak microbeam dose on the film was measured to be 10.4 ± 1.5 Gy with the full width at half maximum of the microbeam created being 260 μm. Based on this measurement, the device should be capable of a $\sim$2 Gy/s in-pulse dose rate with all five cathodes turned on simultaneously.

In addition, a sample PVDR was measured by irradiating a film sandwiched between two 0.5 in. slabs of tissue-equivalent plastic with four separate microbeams created by successively translating the sample stage by 1.4 mm every 15 min for a total of 60 min. For this experiment, the device was operated at an anode voltage of 156 kV, while given a tube current of 14 mA from two cathodes simultaneously run at a 10% duty cycle and 1 ms pulse width. The results, as can be seen in Figure 7(a), yielded a PVDR of $>$17 and a slightly wider beam width of 315 μm. This was to be expected because the film was placed slightly further from the collimator due to the plastic phantom. Based on this measurement, we conclude that our compact CNT-MRT device can achieve relative dose distributions in small animals that are similar to those experimented with at synchrotron facilities.

We have also gone on to verify the capability of the system to deliver MRT in mice. In one preliminary study, a mouse pup (postnatal day 12, P12) was immobilized using a custom-made stereotactic head frame and nose cone, anesthetized using an isoflurane vaporizer from SurgiVet® (Smiths Medical, Norwell, MA), and monitored with the BioVet® system (M2M Imaging, Cleveland, OH). Five 300 μm wide microbeams with a 13 Gy peak entrance dose spaced at 900 μm center to center were delivered to the cerebellum during a 50 min irradiation. The animal was sacrificed 4 h after irradiation. Afterwards, its brain was removed, fixed in paraffin, sliced, and stained for the γ-H2AX foci, a standard marker used to examine DNA damage and subsequent repair of DNA double strand breaks.[33] Figure 7(b) shows the γ-H2AX staining on the P12 mouse brain, clearly indicating radiation-induced DNA damage along the microbeam path. With this animal model and immunohistological technique, it is shown

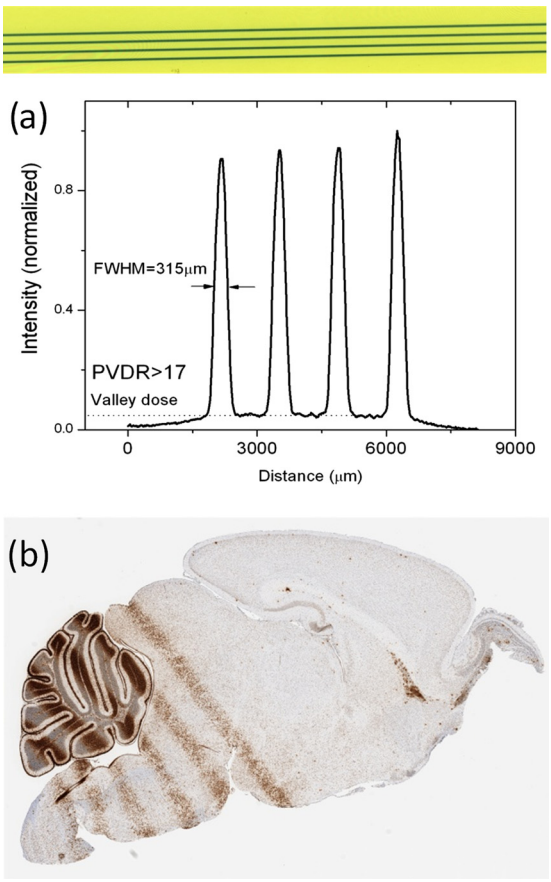

FIG. 7. (a) Irradiated film and dose profile displaying our peak to valley dose ratio given a center to center separation of 1.4 mm between the microbeams. (The intensity variation seen here is due to slight non-uniformity in focal line position and collimator transmission under tube heating during continual use.) (b) Histological image of microbeam DNA damage in a mouse brain. Cell staining was done with γ-H2AX labeling, and the peak entrance dose given was 13 Gy per microbeam.

here that our device is capable of delivering prescribed microbeam radiation dose *in vivo* and enabling further exploration of the effects of microbeam radiation in live animals.

In conclusion, a compact MRT device for radiobiological, mechanistic studies in small animals has been created. Using CNT X-ray technology, this device employs a long focal line to distribute heat across a stationary anode, which allows the generation of high flux X-radiation from the narrow line. We have developed a collimator and alignment system to shape the high flux from the focal line into a single $\sim$300 μm wide microplanar beam. We have demonstrated that this system is capable of producing MRT dose distributions in phantoms and mice comparable to those achieved with synchrotron based MRT systems, and demonstrated the long-term stability needed for mechanistic studies. Using this device, we hope to bring MRT research to the greater scientific community and possibly provide the groundwork for the creation of a clinical scale device.

The authors would like to thank Dr. Guohua Cao for helpful discussions during preliminary device design and Christy Inscoe, Pavel Chtcheprov, Rachel Ger, and Torsten Schreiber for their help with construction, testing, and running of the device. The authors would also like to thank Dr. Timothy Gershon for supplying the mouse pup for experimentation and Andrew Crowther for performing the histological analysis. This work was supported by the Carolina Center of Cancer Nanotechnology Excellence (Grant No. U54-CA151652) and the National Institute of Health Grand Opportunities "GO" program (Grant No. RC2-CA148487).

[1]D. R. Smart, *Physician Characteristics and Distribution in the US 2010* (American Medical Association, Chicago, IL, 2009).
[2]E. J. Hall and A. J. Giaccia, *Radiobiology for the Radiologist*, 6th ed. (Lippincott Williams and Wilkins, Philadelphia, PA, 2006).
[3]J. Van Dyk, "The modern technology of radiation oncology," in *A Compendium for Medical Physicists and Radiation Oncologists* (Medical Physics Publishing, Madison, WI, 2005).
[4]J. A. Laissue, G. Geiser, P. O. Spanne, F. A. Dilmanian, J.-O. Gebbers, M. Geiser, X.-Y. Wu, M. S. Makar, P. L. Micca, M. M. Nawrocky *et al.*, Int. J. Cancer **78**(5), 654 (1998); E. Brauer-Krisch, R. Serduc, E. A. Siegbahn, G. Le Duc, Y. Prezado, A. Bravin, H. Blattmann, and J. A. Laissue, Mutat Res. **704**(1–3), 160 (2010).
[5]F. A. Dilmanian, T. M. Button, G. Le Duc, N. Zhong, L. A. Pena, J. A. L. Smith, S. R. Martinez, T. Bacarian, J. Tammam, B. Ren *et al.*, J. Neuro-Oncol. **4**(1), 26 (2002).
[6]P. Romanelli and A. Bravin, Neurol. Res. **33**(8), 825 (2011).
[7]H. J. Curtis, Radiat. Res. Suppl. **7**, 250 (1967).
[8]W. Zeman, H. J. Curtis, and C. P. Baker, Radiat. Res. **15**(4), 496 (1961).
[9]K. M. Prise and G. Schettino, Radiat. Prot. Dosim. **143**(2–4), 335 (2011).
[10]A. S. Meigooni, U. Malik, H. Zhang, S. A. Dini, N. J. Meigooni, K. Komanduri, and M. Mohiuddin, Iran. J. Radiat. Res. **2**(4), 167 (2005).
[11]W. V. Tenzel, Radiology **59**(3), 399 (1952).
[12]G. Neuner, M. M. Mohiuddin, N. V. Walde, O. Goloubeva, J. Ha, C. X. Yu, and W. F. Regine, Int. J. Radiat. Oncol., Biol., Phys. **82**(5), 1642 (2012).
[13]M. Mohiuddin, M. Fujita, W. F. Regine, A. S. Megooni, G. S. Ibbott, and M. M. Ahmed, Int. J. Radiat. Oncol., Biol., Phys. **45**(3), 721 (1999); J. A. Penagaricano, R. Griffin, P. Corry, E. Moros, Y. Yan, and V. Ratanatharathorn, J. Ark. Med. Soc. **105**(11), 263 (2009).
[14]D. N. Slatkin, P. Spanne, F. A. Dilmanian, and M. Sandborg, Med. Phys. **19**(6), 1395 (1992).
[15]M. De Felici, R. Felici, M. S. del Rio, C. Ferrero, T. Bacarian, and F. A. Dilmanian, Med. Phys. **32**(8), 2455 (2005); J. C. Crosbie, I. Svalbe, S. M. Midgley, N. Yagi, P. A. Rogers, and R. A. Lewis, Phys. Med. Biol. **53**(23), 6861 (2008).
[16]P. Regnard, G. Le Duc, E. Brauer-Krisch, I. Tropres, E. A. Siegbahn, A. Kusak, C. Clair, H. Bernard, D. Dallery, J. A. Laissue *et al.*, Phys. Med. Biol. **53**(4), 861 (2008).
[17]J. A. Laissue, H. Blattmann, M. D. Michiel, D. N. Slatkin, N. Lyubimova, R. Guzman, W. Zimmermann, S. Birrer, T. Bley, P. Kircher *et al.*, Proc. SPIE **4508**, 65 (2001).
[18]F. A. Dilmanian, G. M. Morris, G. Le Duc, X. Huang, B. Ren, T. Bacarian, J. C. Allen, J. Kalef-Ezra, I. Orion, E. M. Rosen *et al.*, Cell. Mol. Biol. (Paris) **47**(3), 485 (2001).
[19]J. A. Laissue, N. Lyubimova, H.-P. Wagner, D. W. Archer, D. N. Slatkin, M. Di Michiel, C. Nemoz, M. Renier, E. Brauer, P. O. Spanne *et al.*, Proc. SPIE **3770**, 38 (1999).
[20]E. A. Siegbahn, J. Stepanek, E. Braüuer-Krisch, and A. Bravin, Med. Phys. **33**(9), 3248 (2006).
[21]D. J. Anschel, A. Bravin, and P. Romanelli, Neurosurg. Rev. **34**(2), 133 (2011).
[22]F. Verhaegen, P. Granton, and E. Tryggestad, Phys. Med. Biol. **56**(12), R55 (2011).
[23]K. Huang, K. Yan, T. Podder, Y. Hu, and Y. Yu, "Feasibility Analysis On Converting Conventional Orthovoltage Biological Irradiator to a Micro-Beam Array for Small Animal/cell Irradiation," paper presented at the AAPM Annual Meeting, Anaheim, CA, 2009 (unpublished).
[24]E. Braüer-Krisch, H. Requardt, T. Brochard, G. Berruyer, M. Renier, J. A. Laissue, and A. Bravin, Rev. Sci. Instrum. **80**(7), 074301 (2009); H. Nettelbeck, G. J. Takacs, M. L. F. Lerch, and A. B. Rosenfeld, Med. Phys. **36**(2), 447 (2009).
[25]J. C. Crosbie, R. L. Anderson, K. Rothkamm, C. M. Restall, L. Cann, S. Ruwanpura, S. Meachem, N. Yagi, I. Svalbe, R. A. Lewis *et al.*, Int. J. Radiat. Oncol., Biol., Phys. **77**(3), 886 (2010); A. Bouchet, B. Lemasson, G. Le Duc, C. Maisin, E. Brauer-Krisch, E. A. Siegbahn, L. Renaud, E. Khalil, C. Remy, C. Poillot *et al.*, Int. J. Radiat. Oncol., Biol., Phys. **78**(5), 1503 (2010).
[26]O. Zhou and X. Calderon-Colon, in *Carbon Nanotube and Related Field Emitters*, edited by Y. Saito (John Wiley and Sons, Hoboken, NJ, 2010), p. 417; G. Cao, Y. Z. Lee, R. Peng, Z. Liu, R. Rajaram, X. Calderon-Colon, L. An, P. Wang, T. Phan, and S. Sultana *et al.*, Phys. Med. Biol. **54**(8), 2323 (2009); X. Qian, A. Tucker, E. Gidcumb, J. Shan, G. Yang, X. Calderon-Colon, S. Sultana, J. Lu, O. Zhou, and D. Spronk *et al.*, Med. Phys. **39**(4), 2090 (2012).
[27]X. Calderon-Colon, H. Geng, B. Gao, L. An, G. Cao, and O. Zhou, Nanotechnology **20**(32), 325707 (2009).
[28]S. Sultana, X. Calderón-Colón, G. Cao, O. Zhou, and J. Lu, Proc. SPIE **7622**, 76225G (2010); J. Zhang, M. Hadsell, J. Lu, O. Zhou, and S. Chang, Proc. SPIE **8668**, 86685C (2013).
[29]J. Shan, O. Zhou, and J. Lu, Proc. SPIE **8313**, 83130O (2012).
[30]*Characteristics of Focal Spots in Industrial X-ray Systems for use in Non-Destructive Testing* (European Committee for Standardization, Brussels, 1999), Vol. EN 12543–5.
[31]*Gafchromic EBT2: Self-Developing Film for Radiotherapy Dosimetry* (International Specialty Products, Wayne, NJ, 2010).
[32]D. Lewis, *Using Radiochromic Film: Tips and Techniques* (International Specialty Products, Wayne, NJ, 2010).
[33]L. J. Kuo and L.-X. Yang, In Vivo **22**(3), 305 (2008).